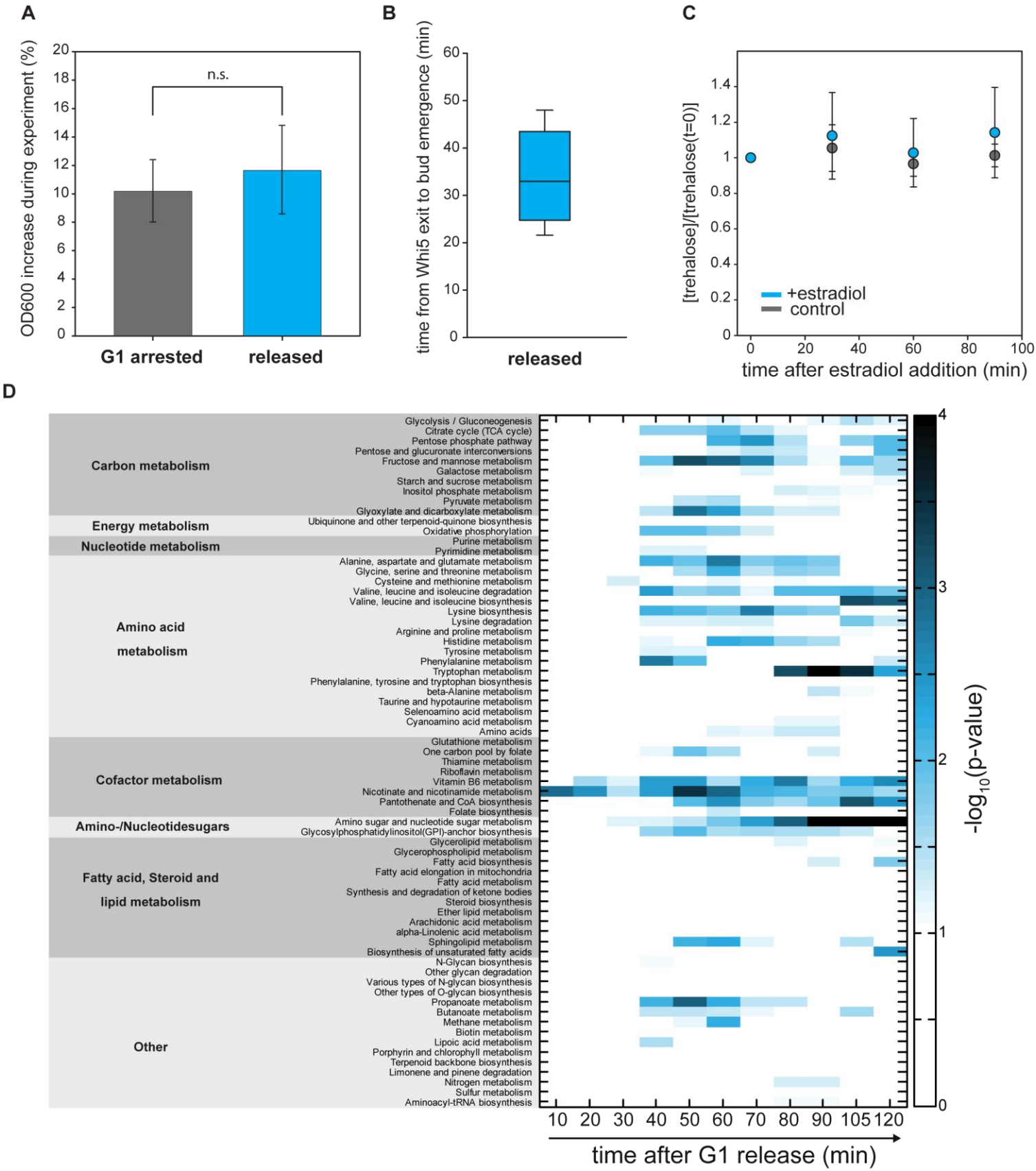
A
OD600 increase during experiment (%)
n.s.
G1 arrested
released
B
time from Whi5 exit to bud emergence (min)
released
C
[trehalose]/[trehalose(t=0)]
+estradiol
control
time after estradiol addition (min)
D
Carbon metabolism
Glycolysis / Gluconeogenesis
Citrate cycle (TCA cycle)
Pentose phosphate pathway
Pentose and glucuronate interconversions
Fructose and mannose metabolism
Galactose metabolism
Starch and sucrose metabolism
Inositol phosphate metabolism
Pyruvate metabolism
Glyoxylate and dicarboxylate metabolism
Energy metabolism
Ubiquinone and other terpenoid-quinone biosynthesis
Oxidative phosphorylation
Nucleotide metabolism
Purine metabolism
Pyrimidine metabolism
Amino acid metabolism
Alanine, aspartate and glutamate metabolism
Glycine, serine and threonine metabolism
Cysteine and methionine metabolism
Valine, leucine and isoleucine degradation
Valine, leucine and isoleucine biosynthesis
Lysine biosynthesis
Lysine degradation
Arginine and proline metabolism
Histidine metabolism
Tyrosine metabolism
Phenylalanine metabolism
Tryptophan metabolism
Phenylalanine, tyrosine and tryptophan biosynthesis
beta-Alanine metabolism
Taurine and hypotaurine metabolism
Selenoamino acid metabolism
Cyanoamino acid metabolism
Amino acids
Cofactor metabolism
Glutathione metabolism
One carbon pool by folate
Thiamine metabolism
Riboflavin metabolism
Vitamin B6 metabolism
Nicotinate and nicotinamide metabolism
Pantothenate and CoA biosynthesis
Folate biosynthesis
Amino-/Nucleotidesugars
Amino sugar and nucleotide sugar metabolism
Glycosylphosphatidylinositol(GPI)-anchor biosynthesis
Fatty acid, Steroid and lipid metabolism
Glycerolipid metabolism
Glycerophospholipid metabolism
Fatty acid biosynthesis
Fatty acid elongation in mitochondria
Fatty acid metabolism
Synthesis and degradation of ketone bodies
Steroid biosynthesis
Ether lipid metabolism
Arachidonic acid metabolism
alpha-Linolenic acid metabolism
Sphingolipid metabolism
Biosynthesis of unsaturated fatty acids
Other
N-Glycan biosynthesis
Other glycan degradation
Various types of N-glycan biosynthesis
Other types of O-glycan biosynthesis
Propanoate metabolism
Butanoate metabolism
Methane metabolism
Biotin metabolism
Lipoic acid metabolism
Porphyrin and chlorophyll metabolism
Terpenoid backbone biosynthesis
Limonene and pinene degradation
Nitrogen metabolism
Sulfur metabolism
Aminoacyl-tRNA biosynthesis
time after G1 release (min)
-log10(p-value)

Figure S1, related to Figure 1: Cell cycle progression following synchronous release from G1 arrest. (A) Cells were arrested in G1 using a hormone inducible *CLN1* allele expressed in cells lacking other G1 cyclins as described in Figure 1A (*LexApr-CLN1 cln1*Δ*cln2*Δ*cln3*Δ). Growth (as determined by OD600 at 5 minutes and 105 minutes after treatment) of cells that were released into the cell cycle (blue) by addition of estradiol or cells that were mock treated and remained G1 arrested (grey). Error bars denote standard deviations from four replicate experiments. (B) Cells expressing Whi5-GFP were arrested in G1 as in A, but were then transferred to an agar patch containing media and estradiol for release. Cells were imaged every 3 minutes and the time between Whi5 exit from the nucleus and bud emergence was determined. N=25 cells. Bars and whiskers denote 5^{th}, 25^{th}, median, 75^{th}, and 95^{th} percentiles. (C) The trehalose pathway is sensitive to stress and increased trehalose concentrations indicate a stress response. To ensure that addition of estradiol does not lead to a stress response, wild type cells, which do not contain any estradiol responsive elements, were grown over night. Cultures were split and one half was treated with 200 nM estradiol (cyan circles), while the other half was mock treated with solvent only. Trehalose concentrations per biomass were determined and normalized to 1 at t= 0 minutes. Error bars denote standard deviations from two biological and two technical replicates. (D) Metabolic pathway enrichment analysis of metabolome data was performed using a hypergeometric test on significantly changing metabolites (q-value < 0.01, $|\log_2(\text{foldchange})| > 0.2$) for a univariate comparison between measurements before and after release into the cell cycle (see experimental procedures for more details).

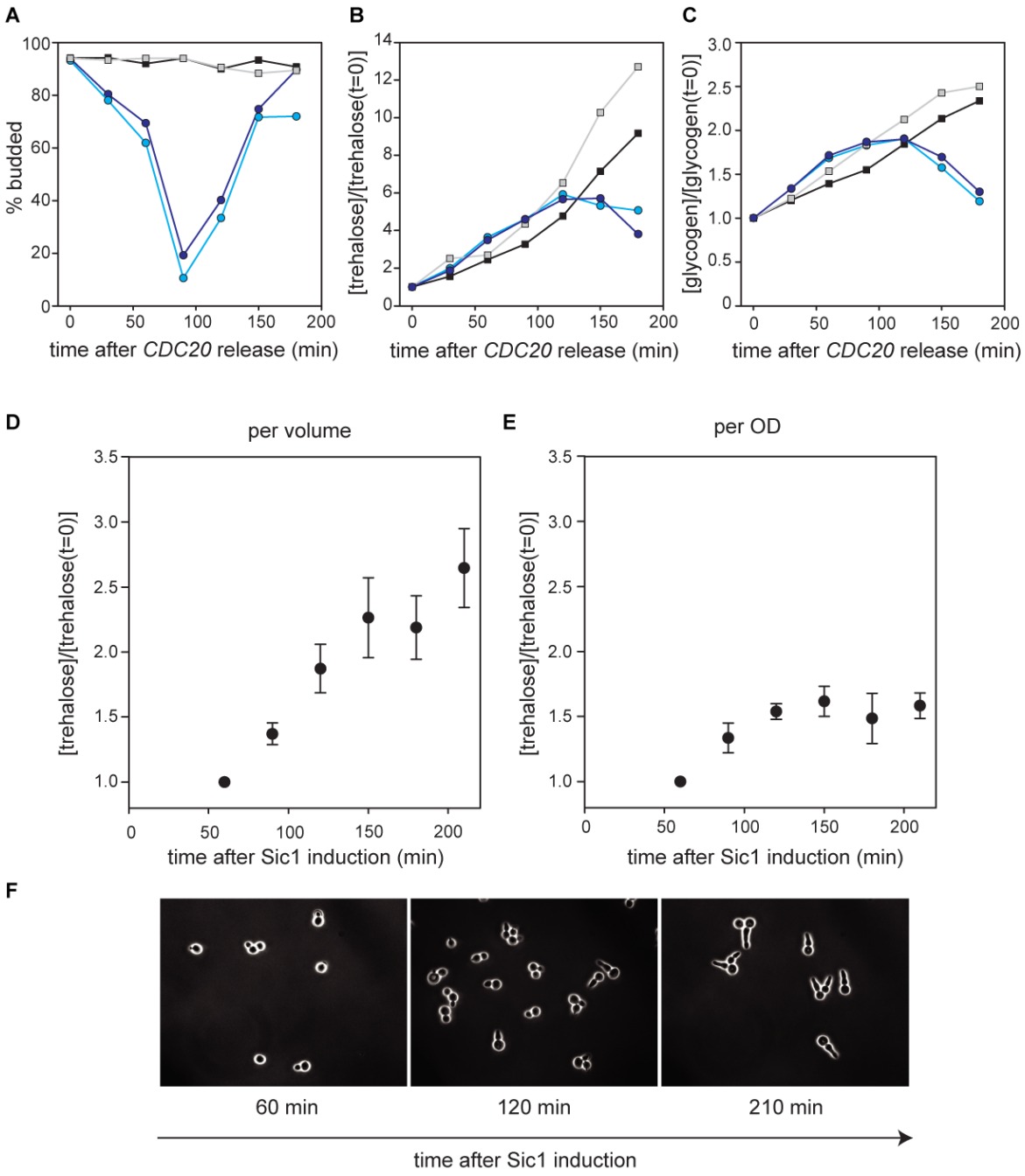

Figure S2, related to Figure 2: Storage carbohydrate concentrations in cells synchronously released from a mitotic arrest. (A) Budding index, (B) trehalose, and (C) glycogen concentrations after a release from mitotic arrest (*LexApr-CDC20*). Blue: released cells; grey: arrested cells. These are two replicates of the experiment as reported in Figure 2E-H in lower time resolution, but now including arrested control cells. Surprisingly, cells arrested in mitosis accumulate storage carbohydrates, despite high Cdk1 activity. This is most likely due to a stress response triggered by the arrest. However, utilization of storage begins at the G1/S transition of the next cell cycle, consistent with storage utilization being activated downstream of *Start*. (D) and (E) Trehalose concentrations following a Sic1 overexpression arrest**.** A *MET3*-promoter was used to induce the expression of a non-degradable truncated Sic1 (Koivomagi et al., 2011a), an inhibitor of B-type cyclin-Cdk1 complexes. (A) trehalose concentration per volume of culture (which does not consider dilution by growth) (B) trehalose concentrations normalized by optical density (C) phase image showing arrested cells

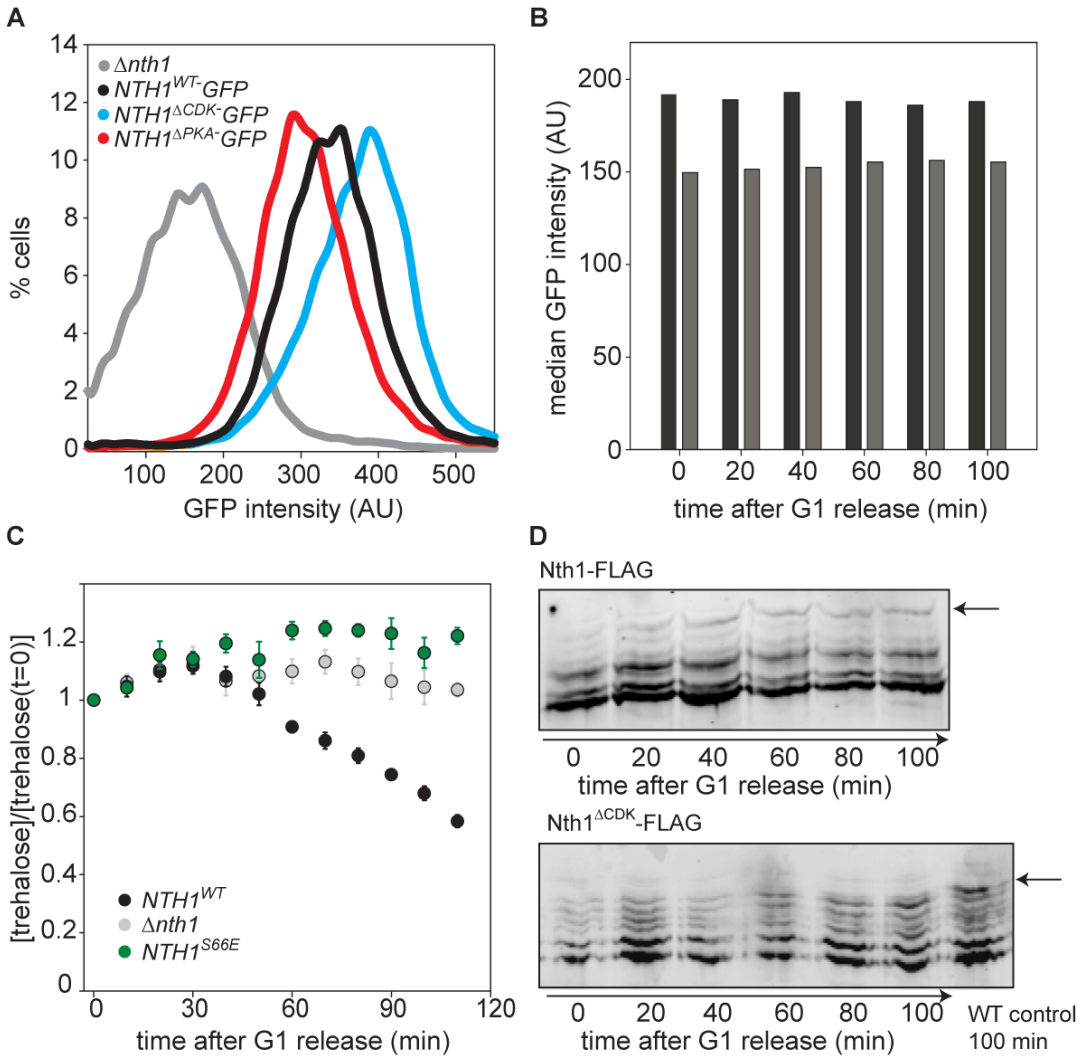

Figure S3, related to Figure 3 and 4: (A) Expression of wildtype and phosphorylation-site mutant alleles in asynchronous culture. *NTH1-GFP* alleles with point mutations in Cdk1 or PKA phosphorylation sites were integrated into *cln1*Δ*cln2*Δ*cln3*Δ *LexApr-CLN1 nth1*Δ strains (see Figure 1 and 2 and Table S3). These cells were grown asynchronously on hormone containing ethanol minimal medium and their Nth1-GFP concentrations were determined by flow cytometry. (B) Nth1-GFP concentrations following release from a G1 arrest. Two different clones of Nth1-GFP were arrested and released as described in Figure 1 and S1 and their fluorescence determined by flow cytometry. A wild type strain without GFP was also released from G1 and was used for subtraction of the autofluorescence background. (C) S66E mutation prevents activation of Nth1 during S/G2/M. *NTH1*^{S66E} cells were arrested in G1 and released into the cell cycle at t=0 minutes as described in Figure 1 and Figure 2A-D. All trehalose concentrations were normalized to the concentration at t=0 minutes. See Table S1 for absolute concentration. Error bars denote the standard error of the mean for two biological replicates with two technical replicates each for *NTH1*^{S66E} and three biological replicates for *nth1*Δ and *NTH1*^{WT}, respectively. Grey denotes *nth1*Δ*nth2*Δ*gph1*Δ, black and green denote wild type *NTH1* and *NTH1*^{S66E} alleles, respectively, in an *nth2*Δ*gph1*Δ background**.** *nth1*Δ and *NTH1*^{WT} are the same data as shown in Figure 4. (D) The fraction of highly phosphorylated Nth1 increases after a release from G1. Cells were released from G1 (see Figure 1 and 2) and samples taken every 20 minutes. Cell lysates were separated on a Phostag-SDS-polyacrylamide gel and Nth1-3xFLAG was detected using Western blot analysis. Representative blots of Nth1-FLAG (top) and Nth1$^{\Delta CDK}$ (bottom) are shown here. The band corresponding to the most highly phosphorylated form of Nth1 (see arrow) was quantified as a fraction of the total signal in the sample (Figure 4D). That the fraction of highly phosphorylated active Nth1 remains fairly low throughout the cell cycle is in good agreement with the very gradual decrease in trehalose concentrations during S/G2/M (Figure 2).

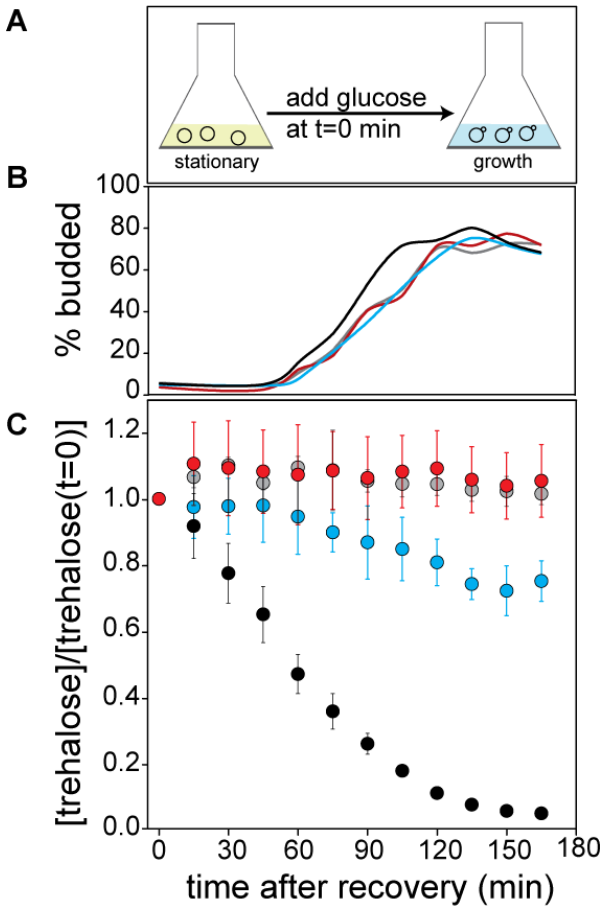

Figure S4, related to Figure 4: Cdk1 and PKA1 phosphorylation are required for Nth1 activation following release from stationary phase. (A) Experiment schematic: cells were grown on glucose minimal medium until reaching stationary phase. Three days after the initial inoculation, cells were diluted into 1% glucose minimal medium. (B) Budding index, and (C), normalized trehalose concentration for cells recovering from stationary phase after transfer to 1% glucose minimal medium at t=0 minutes. Error bars denote the standard error of the mean for two biological replicates with two technical replicates each. All trehalose concentrations were normalized to the concentration at t=0 minutes. Grey denotes *nth1*Δ*nth2*Δ*gph1*Δ, black, blue and red denote wild type *NTH1*, *NTH1*$^{\Delta PKA}$, and *NTH1*$^{\Delta CDK}$ alleles, respectively, in an *nth2*Δ*gph1*Δ background.

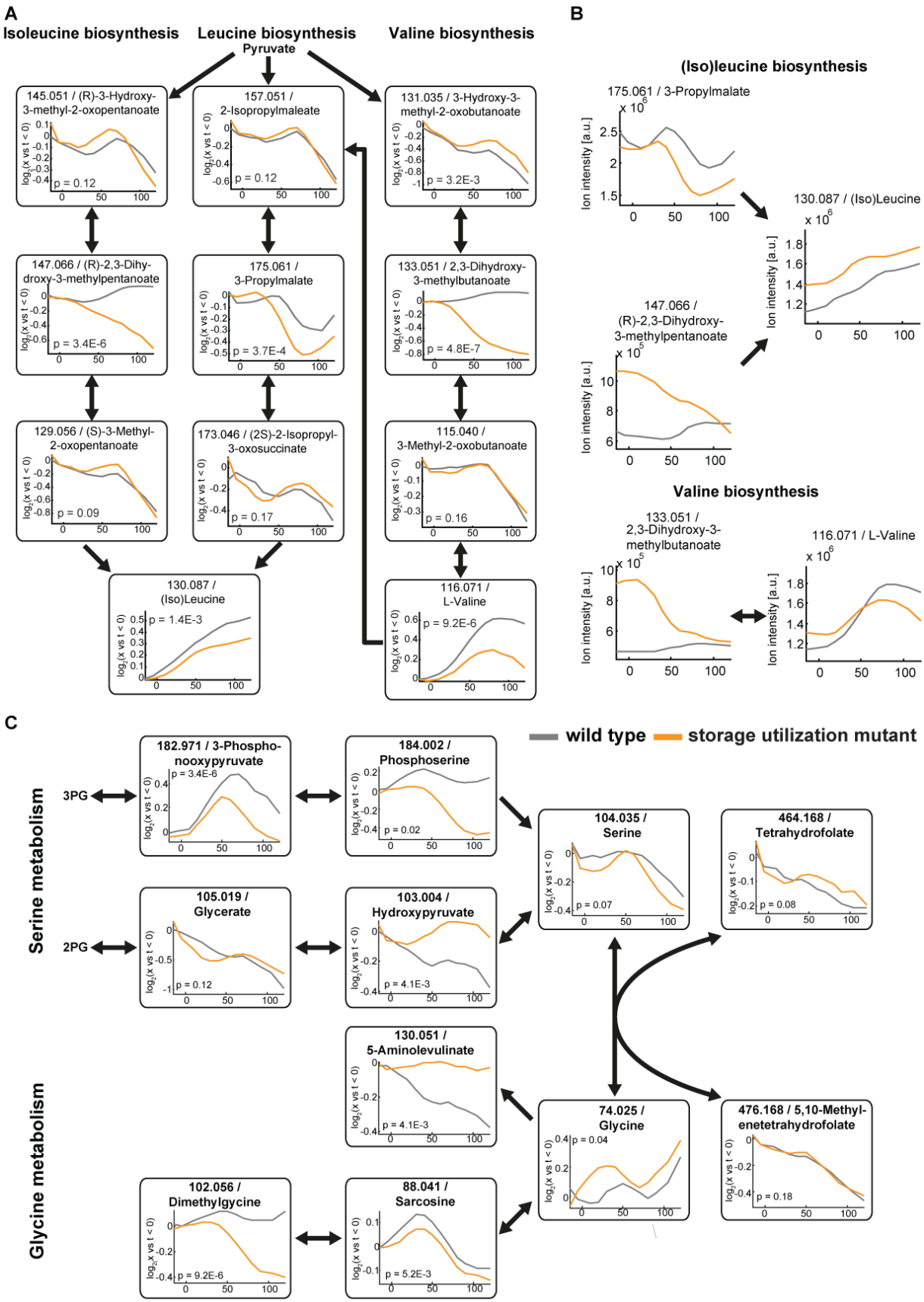
A
Isoleucine biosynthesis
Leucine biosynthesis
Valine biosynthesis
Pyruvate
145.051 / (R)-3-Hydroxy-3-methyl-2-oxopentanoate
p = 0.12
157.051 / 2-Isopropylmaleate
p = 0.12
131.035 / 3-Hydroxy-3-methyl-2-oxobutanoate
p = 3.2E-3
147.066 / (R)-2,3-Dihydroxy-3-methylpentanoate
p = 3.4E-6
175.061 / 3-Propylmalate
p = 3.7E-4
133.051 / 2,3-Dihydroxy-3-methylbutanoate
p = 4.8E-7
129.056 / (S)-3-Methyl-2-oxopentanoate
p = 0.09
173.046 / (2S)-2-Isopropyl-3-oxosuccinate
p = 0.17
115.040 / 3-Methyl-2-oxobutanoate
p = 0.16
130.087 / (Iso)Leucine
p = 1.4E-3
116.071 / L-Valine
p = 9.2E-6
B
(Iso)leucine biosynthesis
175.061 / 3-Propylmalate
130.087 / (Iso)Leucine
147.066 / (R)-2,3-Dihydroxy-3-methylpentanoate
Valine biosynthesis
133.051 / 2,3-Dihydroxy-3-methylbutanoate
116.071 / L-Valine
Ion intensity [a.u.]
C
wild type
storage utilization mutant
Serine metabolism
Glycine metabolism
3PG
2PG
182.971 / 3-Phospho-nooxypyruvate
p = 3.4E-6
184.002 / Phosphoserine
p = 0.02
104.035 / Serine
p = 0.07
464.168 / Tetrahydrofolate
p = 0.08
105.019 / Glycerate
p = 0.12
103.004 / Hydroxypyruvate
p = 4.1E-3
130.051 / 5-Aminolevulinate
p = 4.1E-3
74.025 / Glycine
p = 0.04
476.168 / 5,10-Methyl-enetetrahydrofolate
p = 0.18
102.056 / Dimethylglycine
p = 9.2E-6
88.041 / Sarcosine
p = 5.2E-3

Figure S5, related to Figure 5: (A) Relative metabolite concentration changes comparing wild type and storage mutant cells of metabolites involved valine, leucine and isoleucine biosynthesis. (B) Ion intensities of metabolites in valine, leucine and isoleucine biosynthesis. In contrast to wild type cells (grey), storage utilization mutants (orange) accumulate precursors of isoleucine and valine during a G1 arrest, which are utilized during S and M phases. (Iso)Leucine refers to the sum of Isoleucine and Leucine. (C) Relative metabolite fold-changes of metabolites involved in glycine serine and threonine metabolism. Compared with wild type cells (grey), storage utilization mutants (orange) accumulate precursors of glycine and serine biosynthesis during G1 arrest, which are utilized during S and M phases. Temporal profiles are mean values of two individual biological and two technical replicates.

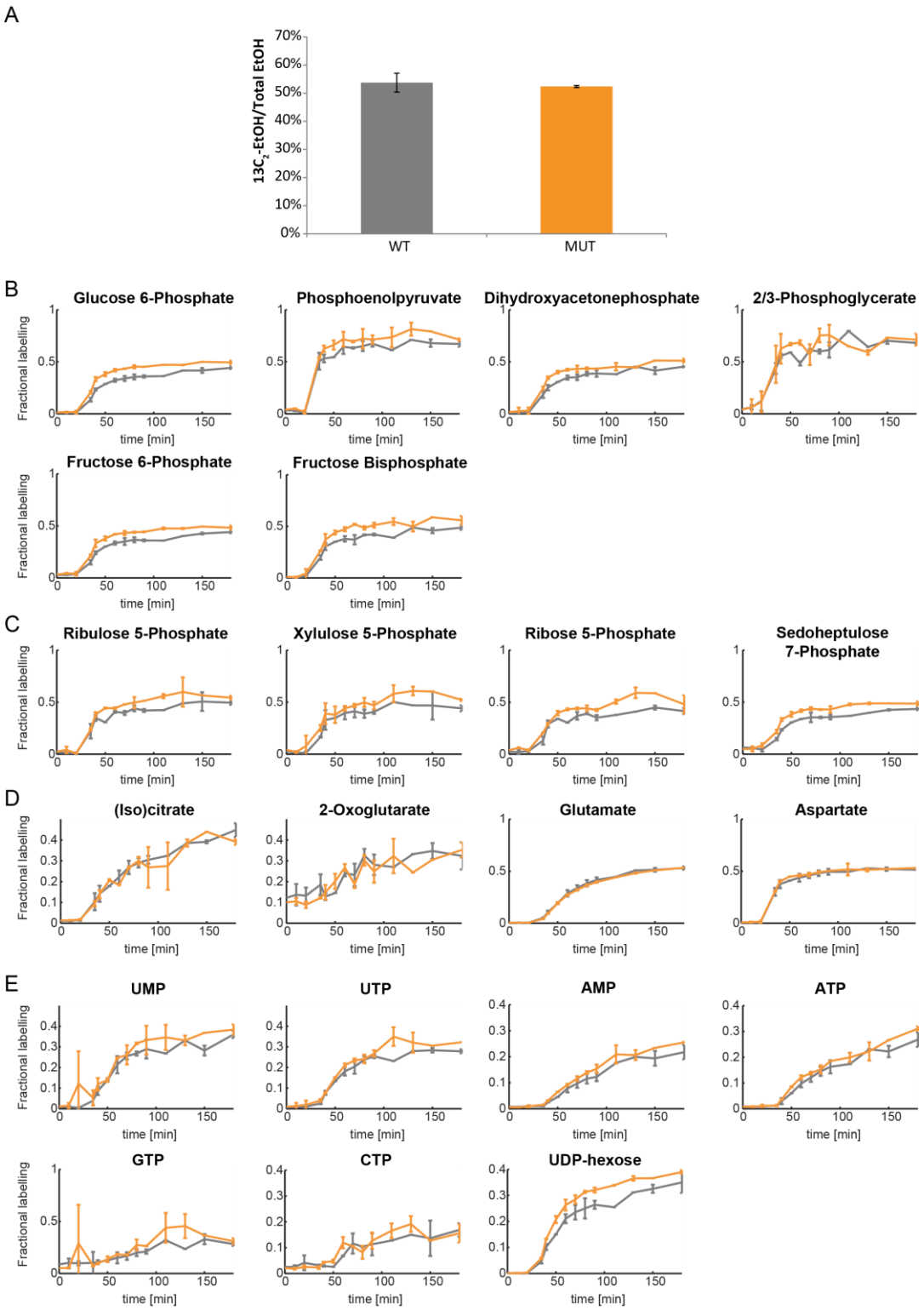

Figure S6, related to Figure 5: Differences in fractional labelling derived by [1,2-13C]-EtOH carbon tracing experiments and targeted metabolomics. (A) Ratio of fully 13C labeled ethanol to total ethanol immediately after addition of [1,2-^{13}C]-EtOH. **(B-E)** Targeted metabolomics derived fractional labeling of metabolites in **(B)** glycolysis, **(C)** pentose phosphate pathway, **(D)** TCA cycle, and **(E)** nucleotide and nucleotide sugar metabolism. Temporal profiles are means of two individual biological replicates, error bars denote standard deviations from two biological and two technical replicates.

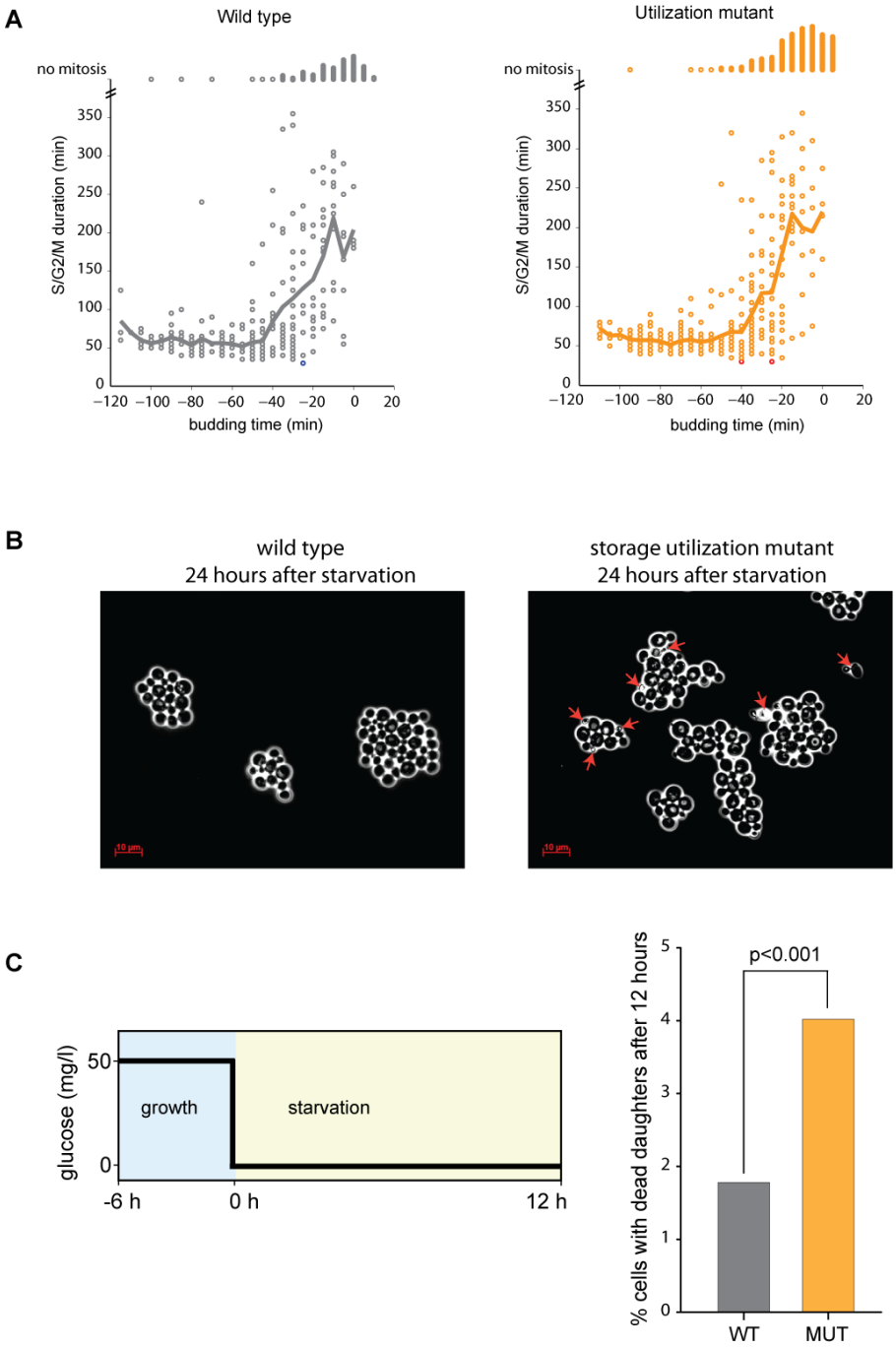

Figure S7, related to Figure 7: Cell cycle response to acute starvation. (A) Wild type (grey) and storage mutant (orange) cells were grown on 50 mg/l glucose minimal medium in a microfluidic imaging platform and subjected to a drop to 0 mg/l glucose (Fig. 7) at t=0 minutes. Htb2-mCherry (fluorescently labeled histone) was used to determine timing and completion of mitosis (see Fig. 7A). S/G2/M was determined as the time from bud emergence to separation of nuclei. Each data point represents one cell, the solid line represents the average for each budding time relative to the starvation, but excluding those cells that failed to complete the cell cycle. Circles at the top of each plot represent those cells that did not complete mitosis by the end of the imaging period, 5.5 hours after the nutrient shift. (B) representative images of wild type and mutant cells 24 hours after the nutrient downshift (C) Quantification of cells with dead progeny 12 hours after nutrient removal. All cells from 12 fields of view (>1200 cells) were counted and the fraction of cells with dead buds from wild type and mutant cells was determined. p-values were calculated using a Fisher's exact test.

Table S1, related to Figures 2,4, and S3,4: Concentrations of trehalose and glycogen

Experiment/ Figure	starting OD	starting concentration of trehalose nmol glucose/ OD600	starting concentration of glycogen nmol glucose/ OD600
G1 release Figure 2			
replicate 1	0.6	280	180
replicate 2	0.55	210	110
replicate 3	0.68	230	110
replicate 4	1	305	110
mean		256	128
G1 release Figure 4A-B			
*nth1*Δ	0.4	180	ND
*nth1*Δ	0.66	192	ND
*nth1*Δ	0.3	156	ND
mean		176	
NTH1	0.2	136	ND
NTH1	0.43	158	ND
NTH1	0.49	176	ND
mean		157	
NTH1$^{\Delta CDK}$	0.31	110	ND
NTH1$^{\Delta CDK}$	0.43	184	ND
NTH1$^{\Delta CDK}$	0.66	220	ND
mean		171	
NTH1 $^{\Delta PKA}$	0.27	116	ND
NTH1 $^{\Delta PKA}$	0.32	130	ND
NTH1 $^{\Delta PKA}$	0.55	148	ND
mean		131	
G1 release Figure S3C			
NTH1$^{\Delta S66E}$	0.62	171	ND
NTH1$^{\Delta S66E}$	0.61	174	ND
mean		173	
recovery from stationary phase Figure S4			
*nth1*Δ	0.6	342	ND
*nth1*Δ	0.55	473	ND
mean		407	
NTH1	0.62	407	ND
NTH1	0.55	332	ND
mean		370	
NTH1$^{\Delta CDK}$	0.59	483	ND
NTH1$^{\Delta CDK}$	0.53	408	ND
mean		445	
NTH1 $^{\Delta PKA}$	0.58	319	ND
NTH1 $^{\Delta PKA}$	0.54	522	ND
mean		420	

Table S2, related to Figure 3 and 4: Cell cycle dependent phosphorylation of enzymes in storage carbohydrate metabolism. We list all enzymes of the trehalose and glycogen pathways in yeast and whether they have been identified to be cell cycle regulated by U: (Ubersax et al., 2003), or H:(Holt et al., 2009). We further queried the phosphogrid database (phosphogrid.org) whether these sites had been detected in other phosphoproteomics datasets (5th column).

Enzyme	Gene Name	Found to be CDK regulated?	SP sites regulated	SP identified in how many other data sets (phosphogrid.org)?
trehalose synthesis				
Tps1	YBR126C	-	-	-
Tps3	YMR261C	H	S148	7
Tsl1	YML100W	H	S77,S135,S147,S161	8,4,6,6
Tps2	YDR074W	H	-	-
trehalose utilization				
Nth1	YDR001C	U,H	S66	4
Nth2	YBR001C	H	-	-
Ath1	YPR026W	-	-	-
glycogen synthesis				
Glg1	YKR058W	-		
Glg2	YJL137C	-		
Gsy1	YFR015C	H	S655	13
Gsy2	YLR258W	H	S655	12
Glc3	YEL011W	H	-	
glycogen utilization				
Gph1	YPR160W	U,H	-	
Gdb1	YPR184W	-	-	

Table S3, related to Experimental Procedures: *Strains used in this study*

name/ experiment	**genotype (all strains are congenic with *S. cerevisiae W303*)**	**comment/ source**
JE621b mitotic arrest Figures 2E-H and S2A-C	*MAT α, his3::LexA-ER-AD-TF- HIS3, cdc20Pr::natMX-LexApr, ADE1, TRP1, LEU2, URA3*	transcription factor was inserted using plasmid FRP880 (Ottoz et al., 2014), the LexA promoter was inserted by PCR cloning based on plasmid FRP793 (Ottoz et al., 2014) (kind gift by Fabian Rudolf, Joerg Stelling lab, Switzerland)
JE611c G1 arrest Figures 1, 2A-C, 5	*MAT α, cln1Δ, cln2Δ, cln3::LEU2, LexAPr-CLN1-LEU2, , his3:: LexA-ER-AD-HIS3, TRP1, ADE2, URA3*	transcription factor was inserted using plasmid FRP880 (Ottoz et al., 2014), the LexA promoter was inserted to replace an existing Gal promoter in a *cln1*Δ, *cln2*Δ, *cln3*::leu2, *GAL1*pr-*CLN*1-*LEU2* strain (lab stock)
JE623c G1 arrest utilization mutant Figures 4-5	*MAT α, cln1Δ, cln2Δ, cln3::LEU2, LexAPr-CLN1-LEU2, ,his3::LexA-ER-AD-HIS3, TRP1, ADE2, URA3, nth1::natMX, nth2::hphMX, gph1::kanMX*	
JE625 G1 arrest *NTH1* Figure 4	*MAT α, cln1Δ, cln2Δ, cln3::leu2, LexAPr-CLN1-LEU2, his3:: LexA-ER-AD-HIS3, TRP1, ADE2, nth1::natMX, gph1::kanMX, , nth2::hphMX, nth1::NTH1pr-NTH1-URA3*	after deletion of *nth1*, a pRS406 plasmid (Stratagene) containing *NTH1* promoter-*NTH1* was integrated into the genomic *NTH1* promoter
JE628 G1 arrest $NTH1^{\Delta CDK}$ Figure 4	*MAT α, cln1Δ, cln2Δ, cln3::leu2, LexAPr-CLN1-LEU2, his3:: LexA-ER-AD-HIS3, TRP1, ADE2, nth1::natMX ,gph1::kanMX, nth2::hphMX, nth1::NTH1pr-NTH1* ^{S66A} *-URA3*	like JE623 above, but *NTH1* S66A
JE627 G1 arrest $NTH1^{\Delta PKA}$ Figure 4	*MAT α, cln1Δ, cln2Δ, cln3::leu2, LexAPr-CLN1-LEU2, his3:: LexA-ER-AD-HIS3, TRP1, ADE2, nth1::natMX , gph1::kanMX, nth2::hphMX, nth1::NTH1pr- NTH1* ^{S20,21,60,83A} *-URA3*	like above, but *NTH1* S20A, S21A, S60A, S83A
JE637 G1 arrest $NTH1^{\Delta S66E}$ Figure S3C	*MAT α, cln1Δ, cln2Δ, cln3::leu2, LexAPr-CLN1-LEU2, his3:: LexA-ER-AD-HIS3, TRP1, ADE2, nth1::natMX, gph1::kanMX, nth2::hphMX, nth1::NTH1pr- NTH1* ^{S20,21,60,83A} *-URA3*	like above, but *NTH1* S66E
JE630 *NTH1-GFP* Figure S3A-B	*MAT α, cln1Δ, cln2Δ, cln3::leu2, LexAPr-CLN1-LEU2, his3:: LexA-ER-AD-HIS3, TRP1, ADE2, nth1::natMX , gph1::kanMX, , nth2::hphMX, nth1::NTH1pr-NTH1-GFP-URA3*	like above but *NTH1-GFP* was added to the plasmid
JE631 $NTH1^{\Delta CDK}$*-GFP* Figure S3A	*MAT α, cln1Δ, cln2Δ, cln3::leu2, LexAPr-CLN1-LEU2, his3:: LexA-ER-AD-HIS3, TRP1, ADE2, nth1::natMX, gph1::kanMX, nth2::hphMX, nth1::NTH1pr-NTH1* ^{S66A} *- GFP -URA3*	like above but $NTH1^{S66A}$ *-GFP* was added to the plasmid
JE632 $NTH1^{\Delta PKA}$*-GFP* Figure S3A	*MAT α, cln1Δ, cln2Δ, cln3::leu2, LexAPr-CLN1-LEU2, his3:: LexA-ER-AD-HIS3, TRP1, ADE2, nth1::natMX , gph1::kanMX, nth2::hphMX, nth1::NTH1pr- NTH1* ^{S20,21,60,83A} *- GFP -URA3*	like above but *NTH1* $^{S20A,S21A, S60A, S83A}$ *-GFP* was added to the plasmid
JE634 *NTH1-3XFLAG* Figures 3,4 and S3D	*MAT α, cln1Δ, cln2Δ, cln3::leu2, LexAPr-CLN1-LEU2, his3:: LexA-ER-AD-HIS3, TRP1, ADE2, nth1::natMX, gph1::kanMX, , nth2::hphMX, nth1::NTH1pr-NTH1-3XFLAG-URA3*	like above but *NTH1-3XFLAG* was added to the plasmid

JE635 *NTH1$^{\Delta CDK}$-3XFLAG* Figures 3,4 and S3D	*MAT α, cln1Δ, cln2Δ, cln3::leu2, LexAPr-CLN1-LEU2, his3:: LexA-ER-AD-HIS3, TRP1, ADE2, nth1::natMX, gph1::kanMX, nth2::hphMX, nth1::NTH1pr-NTH1 ^{S66A} - 3XFLAG -URA3*	like above but *NTH1^{S66A} -3XFLAG* was added to the plasmid
JE636 *NTH1$^{\Delta PKA}$-3XFLAG* Figures 3,4	*MAT α, cln1Δ, cln2Δ, cln3::leu2, LexAPr-CLN1-LEU2, his3:: LexA-ER-AD-HIS3, TRP1, ADE2, nth1::natMX, gph1::kanMX, nth2::hphMX, nth1::NTH1pr- NTH1^{S20,21,60,83A} - 3XFLAG -URA3-*	like above but *NTH1 $^{S20A,S21A, S60A, S83A}$ -3XFLAG* was added to the plasmid
JE401 wild type Figures 6,7, S1C and S7	*MAT* a,*WHI5-GFP*-natMX, *HTB2-mCherry-spHIS5*, *URA3*, *LEU2*, *TRP1*, *ADE2*	
JE225 *nth1*Δ *gph1*Δ utilization mutant Figures 6,7, S4, S7	*MAT* a,*WHI5-GFP*-natMX, *HTB2-mCherry-spHIS5*, *URA3*, *LEU2*, *TRP1*, *ADE2*, *gph1*::kanMX, *nth1*::kanMX, *nth2*::kanMX	
JE226 *NTH1* Figures 7, S4, S7	*MAT* α,*WHI5-GFP*-natMX, *HTB2-mCherry-spHIS5*, *LEU2*, *TRP1*, *ADE2*, *nth1::*kanMX *gph1*::kanMX, *nth2*::kanMX, *nth1*::*NTH1*pr-*NTH1-URA3*	after deletion of *nth1*, a pRS406 plasmid (Stratagene) containing *NTH1* promoter-*NTH1* was integrated into the genomic *NTH1* promoter
JE227 *NTH1$^{\Delta CDK}$* Figures 7, S4, S7	*MAT* α,*WHI5-GFP*-natMX, *HTB2-mCherry-spHIS5*, *LEU2*, *TRP1*, *ADE2*, *nth1::*kanMX *gph1*::kanMX, *nth2*::kanMX, *nth1*::*NTH1*pr-*NTH1 ^{S66A} -URA3*	like above, but *NTH1* S66A
JE228 *NTH1$^{\Delta PKA}$* Figures S4, S7	*MAT* α,*WHI5-GFP*-natMX, *HTB2-mCherry-spHIS5*, *LEU2*, *TRP1*, *ADE2*, *nth1::*kanMX, *gph1*::kanMX, *nth2*::kanMX, *nth1*::*NTH1*pr-*NTH1^{S20,21,60,83A} -URA3*	like above, but *NTH1* S20A, S21A, S60A, S83A
JE216b synthesis mutant Figure 6	*MAT* a, *WHI5-GFP*-natMX, *HTB2-mCherry-spHIS5*, *LEU2*, *TRP1*, *ADE2*,*URA3*, *nth1::*kanMX, *gsy1*::kanMX, *gsy2*::kanMX, *tps1*::kanMX	
JE640 Figure S2	*MAT a, ADE, TRP, HIS, LEU, ura3::MET3 Pr-sic1 ND- URA3*	pRS406 containing *MET3* promoter driving the N-terminal domain of Sic1(Koivomagi et al., 2011a) was intergrated into the *URA3* locus

Table S4 description (Excel Sheet), related to Figures 1 and 5: Metabolite ion intensities after release from G1 for wild type and storage utilization mutant *nth1 nth2 gph1*Δ cells. Complete metabolomics data set including exact m/z values and metabolite assignments for the experiments described in Figure 1, 5, S8-9.

Table S5 description (Excel Sheet), related to Figure 5: Ion intensities of ^{13}C labeled metabolites after addition of [1,2-^{13}C]-ethanol. Wild type and storage utilization mutant *nth1 nth2 gph1*Δ cells were released from a G1 arrest and after 30 minutes [1,2-^{13}C]-ethanol was added so that 50 % of the ethanol in the media was labeled (see methods and Figure S10). Complete metabolomics data set is reported here including exact m/z values and metabolite assignments for all isotopes for the experiments described 5 E-G and S10.

Table S6 description (Excel Sheet), related to Figure 5: Fractional labeling derived by [1,2-^{13}C]-EtOH carbon tracing experiments and targeted metabolomics. Fractional labeling calculated from data reported in Table S5 as described in the experimental procedures.

Movie File 1 description, related to Figure 7: Cell response to a rapid drop in nutrient supply. *HTB2-mCherry*, histone labeled yeast cells were grown on a microfluidics imaging platform in 50 mg/l glucose minimal medium and subjected to a sudden drop to 0 mg glucose. Images were taken every five minutes for 2 hours before and 5.5 hours after the media shift at t=0 minutes. Arrows indicate two cells that were both in S/G2/M when the shift occurs. The top cell completes mitosis, while the bottom cell does not and remains in a budded state.

Supplemental Experimental Procedures

Strains: All strains were constructed using standard methods and are prototrophic in a *Saccharomyces cerevisiae* W303 background. For exogenous control of gene expression we used the recently reported LexA-estrogen-receptor-activation-domain (Lex-ER-AD) system (Ottoz et al., 2014). A plasmid containing the Lex-ER-AD transcription factor sequence was integrated into the *URA3* locus. The sequence for the corresponding *LEXA* promoter was inserted in front of the gene of interest. Estrogen inducible strains were transformed and maintained on YPD plates containing 100 nM β-estradiol (Sigma). *MET3 Pr-sic1ND* strain was maintained on media supplemented with 200 mg/L methionine. See Table S3 for strain genotypes. All constructs were Sanger-sequenced and integrations confirmed by two independent PCRs of genomic DNA.

Media: Yeast nitrogen base minimal media (5 g/l ammonium sulphate, 1.7 g/l YNB (USBiological), pH adjusted to 5, with either 1% ethanol or the specified amount of glucose) was used throughout, except for the mitotic release experiment in Figure 2E-H and the Sic1 arrest experiment in Figure S4, which were performed on 1% ethanol synthetic complete medium (supplemented with 20 amino acids and nucleobases), since LexAPr-Cdc20 cells have trouble recovering from the mitotic arrest on minimal media and the methionine induction of Sic1 does not work well on minimal media. The media used for the starvation experiments was supplemented with sorbitol to avoid changes in osmotic pressure. The glucose minimal medium used for Figure S4 contained 1% glucose and was supplemented with 50 mM potassium phalate to buffer cultures at pH 5.

Cell cycle synchronization: For each experiment, two sequential 24-hour pre-cultures were grown on media containing 10 and 5 nM β-estradiol (Sigma), respectively. To induce cell cycle arrest, cells were filtered, washed and the filter resuspended in estradiol-free medium (starting OD600 was between 0.1 and 0.2). Before release, inducible *LexApr-CDC20* strains were arrested for 6 hours (Figure 2E-H), and inducible *LexApr-CLN1* strains were arrested for 15 hours (all other figures). Cells were released into the cell cycle by addition of 200 nM β-estradiol (dissolved at 1 mM in 100% ethanol). Cell cycle progression was monitored by counting the fraction of budded cells (n > 200 cells per time point). For Figure S2 D-F cells were first grown in media supplemented with 200 mg/L methionine. To induce Sic1-ND expression, cells were filtered and resuspended in methionine-free media.

Metabolite measurements: For metabolite extraction, 1 ml aliquots of yeast cultures grown in shake flasks to an OD of 0.5-0.7 at 600 nm were vacuum filtered on a 0.45 µm pore size polyvinylidene fluoride filter (Millipore). Filters were immediately transferred to 4 ml 70:30 ethanol:water at 75° C for 2 minutes as described in (Link et al., 2013). Metabolite extracts were dried at 0.12 mbar pressure and resuspended in either 50 µl or 100 µl nanopure water. Metabolomics samples were analyzed by flow-injection analysis on an Agilent 6550 Q-TOF (Agilent, Santa Clara, CA) using the following settings (Fuhrer et al., 2011): negative mode; 4 GHz, high resolution mode; scanning the m/z range of 50-1000. Based on exact mass with a tolerance of 0.001 Da and considering $[M\text{-}H^+]$ and $[M+F^-]$ ions, ions were annotated to known metabolites using the KEGG sce database specific for *Saccharomyces cerevisiae* (Kanehisa and Goto, 2000). Since we cannot differentiate between isomers with this method, 562 ions were annotated to 942 metabolites. If not stated otherwise, ion intensities were normalized by a univariate comparison between each individual measurement and the intensities of the 3 time points prior to release from G1 with foldchange = (log2(intensities(t)/intensities(t<0)) using a two-sample t-test, where p-values were corrected for false discovery rate as described in (Storey, 2002). Metabolic pathway enrichment analysis was performed using a hypergeometric test on significantly changing ions (p-value < 0.01, $|\log_2(\text{foldchange})| > 0.2$) of this univariate comparison . We calculated the p-values for a given comparison and pathway with

$$p_{Ptw}(Ptw_{Hits}|Total_{NotHits}, Ptw_{Hits}, Total_{Hits}) = \frac{\binom{Ptw_{NotHits}}{Ptw_{Hits}}\binom{Total_{NotHits} - Ptw_{NotHits}}{Total_{Hits} - Ptw_{Hits}}}{\binom{Total_{NotHits}}{Total_{Hits}}}$$

where $Total_{Hits}$ is the total number of significant ions in the hit subset, $Total_{NotHits}$ is the total number of ions without the hit subset (background), Ptw_{Hits} is the intersection of all ions in the hit subset with ions involved in a given pathway, and $Ptw_{NotHits}$ is the intersection of all background ions with ions involved in a given pathway. The hypergeometric test was applied recursively for each pathway by starting with the most significant ion as a hit followed by increasing the hit subset with the next most significant ion with each iteration. The most significant p-value of this recursive test was considered to represent the probability of metabolic enrichment for a given pathway. To compare metabolite profiles of wild type and storage degradation mutants, we applied a repeated measure ANOVA and corrected the p-values as above for false discovery. Enrichment analysis was performed as described above on significantly changing temporal profiles ($p[group] \leq 0.01$). For plotting, a moving average filter was applied on time profiles of metabolites. All metabolomics data analysis was performed using custom Matlab software (The Mathworks, Natick).

^{13}C ***labeling experiments:*** Yeast cultures were synchronized in G1 as described above. Thirty minutes after release from cell cycle arrest, [U-^{13}C] ethanol (Cambridge Isotope Laboratories, Andover, MA) was added to reach a ratio of 50% naturally labeled/50% fully labeled ethanol (see Fig S.6A). Cells were sampled and intracellular metabolites were extracted as described above. For untargeted analysis, samples were measured as reported previously and ions were annotated to known metabolites in the KEGG sce database (Kanehisa and Goto, 2000) using exact mass with a tolerance of 0.001 Da and considering [M-H^+] and [M+F^-] ions and all possible carbon mass isotopomers. Targeted metabolomics analysis was performed using ultra high-pressure chromatography- tandem mass spectrometry as reported previously (Buescher et al., 2010; Ruhl et al., 2012). Abundance of mass isotopomers for the targeted measurements were corrected for natural occurring abundances of ^{13}C (Yuan et al., 2008). Fractional labeling for each metabolite was calculated with

$$FL = \frac{\sum_{i=0}^{n} i \cdot x_{m+i}}{n}$$

$$x_{m+i} = \frac{int_{m+i}}{\sum_{j=0}^{n} int_{m+j}}$$

where n is the total number of C-atoms and int_{m+i} is the intensity of the (m+i)-ion of a metabolite with i ^{13}C labeled carbon atoms.

Trehalose and glycogen measurements: 1.5 ml of cell culture were chilled on ice for 2 minutes. Cells were centrifuged at 17,000 g for 1 minute and the cell pellets were frozen in liquid nitrogen. For media containing glucose, an additional wash step with 1 ml cold carbon-free medium was performed. Trehalose was extracted by adding 200 µl boiling water to the frozen pellet and placing the sample in a boiling water bath for 10 minutes. During this step, the sample was mixed vigorously every ~2 minutes. Samples were then centrifuged for 5 minutes at 17,000 g and the supernatant collected. This was followed by a second extraction of the pellet. The supernatants were combined and frozen until analysis. The trehalose concentration was determined enzymatically using a commercial kit (K-Treh, Megazyme) and a Tecan plate reader. The glycogen extraction protocol was slightly modified from (Muller et al., 2003): 125 µl 0.25 M sodium carbonate were added to the frozen cell pellet, which was then incubated for four hours at 85˚C. 75 µl 1M acetic acid, 300 µl sodium acetate (200 mM, pH 5.2) and 2 µl amyloglucosidase (from *Aspergillus niger*, Sigma, 1000 U/ml) were then added and samples were incubated at 60˚C overnight. Samples were centrifuged and the supernatants frozen until analysis. Prior to analysis, samples were filtered. Glucose released from glycogen digestion was measured enzymatically using the components from the Megazyme K-Treh kit except the trehalase. For all trehalose and glycogen concentrations reported in Figures 2 and 4, we normalized the amounts measured at each time point (2 technical replicates) to the amount measured in the

sample at t = 0 minutes. Notably, we did not divide by the slightly increasing biomass. Decreasing values in our measurement correspond to net utilization of storage carbohydrates, while a constant value corresponds to concentration dilution by growth. Absolute values (µmol/OD unit) for each experiment are reported in Table S1.

Imaging and image analysis: Images were recorded every 5 minutes (every 3 minutes for Figure S1B) on a Zeiss Axio-Observer Z1 with an automated stage and a plan-apo 63×/1.4NA oil immersion objective. The nuclear marker Htb2-mCherry was expressed from the endogenous locus and its fluorescence was measured using 12 ms exposure with the Colibri 540-80 LED module at 25% power. The cell cycle marker Whi5-GFP was expressed from the endogenous locus and its fluorescence was measured using 400 ms exposure with the Colibri 540-80 LED module at 5% power.

For the experiments described in Figure 7 cells were imaged on a commercial microfluidic system (CellAsic, EMD Millipore) with the flow pressure set to 4 psi. Pre-cultures were grown overnight in 1% galactose minimal medium (non-repressive sugar). Cells were sonicated for 5 s before being loaded into the microfluidic plate at 8psi. Cells were adapted to minimal medium containing 50 mg/l glucose for 5 hours before imaging. Cells were then grown in medium containing 50 mg/l glucose for another 120 minutes during imaging before we switched cells to a medium containing no glucose (50 mg/l sorbitol, which budding yeast cannot metabolize, 0.1X YNB and 5 g/l ammonium sulphate). For Figure 7F cells were grown for 2 hours in 50 mg/L glucose, 0.1X YNB, 5 g/L ammonium sulphate and then for 12 hours in 0 mg/L glucose, 0.1X YNB, 5 g/L ammonium sulphate (no sorbitol).

For the single cell measurements described in Figure 6 and S1 cells were grown on agar patches for imaging since ethanol does not work well with the microfluidic system. 1.5 % agar was melted in 1x YNB and 5g/L ammonium sulphate and ethanol was added to 1% after cooling. Agar was solidified and cut into patches. Cells were grown overnight in ethanol medium, sonicated for 5 s and 1 µl cell suspension was sandwiched between an agar patch and a coverslip. Coverslips were transferred to the microscope and the agar was covered with another coverslip.

Images were processed and cells segmented as described in (Doncic et al., 2013). For Figure 6, only first generation mother cells were scored. For Figure 7 all cells that initiated budding during the 120 minutes of imaging prior to carbon depletion were analyzed. Bud emergence and mitosis (separation of nuclei) were scored visually and annotated using custom MATLAB software. S/G2/M durations were estimated using Whi5 exit and re-entry in Figure 6C, and using bud emergence and separation of nuclei in Figure S7. Cell death was scored visually by a change in morphology, loss in nuclear fluorescence, and an increase in autofluorescence.

DNA content: 1 ml of cell suspension (OD600 ~0.5) was fixed in 9 ml precooled 80% ethanol and incubated overnight. Cells were pelleted by centrifugation and were consecutively washed in 5 ml and 2 ml of Tris-HCl (50 mM, pH8). Cells were treated for 40 minutes with RnaseA (300 µl, 1mg/ml, 37˚C), 60 minutes with Proteinase K (50 µl, 20 mg/ml, 37˚C), and 60 minutes with SYBR Green I (life technologies, 200 µl (1:1000 dilution) at room temperature). Between each incubation, cells were washed twice with 1 ml of Tris-HCl (50 mM, pH8). Stained cells were diluted 1:10 in Tris-HCl and sonicated before analysis. Samples were analyzed on a BD FACSCalibur flow cytometer at 488 nm excitation and 530 (+/-30) nm emission filter.

In vitro phosphorylation assay: N-terminally 6xHis-tagged recombinant Nth1 constructs were expressed in *E. coli* and were purified by cobalt affinity chromatography. *In vitro* phosphorylation assays using purified Clb2/Cdk1/Cks1 complexes were performed as described previously (Koivomagi et al., 2011b). Figure 3B corresponds to an 8 minute *in vitro* reaction.

Phos-tag SDS-PAGE and Western analysis: Cells were sampled and transferred into twice the sample volume of 60% methanol, 20 mM Tris-HCl (pH 7.5) (prechilled to -20˚C) and centrifuged at 4000g. Pellets were frozen in liquid nitrogen and stored at -80˚C. Lysates were prepared using a bead beater in lysis buffer containing 8M urea. To separate the phosphorylated species of Nth1-3xFlag, 8% SDS-polyacrylamide (Biorad 29:1) gels were used. These

were supplemented with the 100 µM Phos-tag reagent (FMS Laboratory, NARD institute, Japan) and 100 µM $MnCl_2$ according to the instructions from the manufacturer. Gels were blotted on a dry system iBlot (Invitrogen) and Nth1-3xFLAG was labeled with ANTI-FLAG M2 antibody (Sigma) and Alexa Fluor 680 goat anti-mouse antibody (Life Technologies). Blots were imaged on a Li-COR Odysseus Imager. Bands were quantified using custom image analysis software in Matlab.

Trehalase activity assay: The trehalase assay was adapted from previously published protocols (Muller et al., 2003; Pernambuco et al., 1996; Uno et al., 1983; Veisova et al., 2012). Cells were synchronized as described above. At specified time points, 20 ml of culture were quenched by pipeting into 80 ml of ice cold wash buffer (50 mM Tris HCl pH7). Cells were pelleted at 4˚C, washed with 1ml of buffer and pelleted again. The supernatant was completely removed and cells were frozen in liquid nitrogen. Cells were lysed by bead beating in 200 µl lysis buffer (50 mM Tris pH7, 50 uM $CaCl_2$, 1 mM DTT, EDTA-free protease and phosphatase inhibitor cocktail (HALT, Thermo Scientific)). Crude extracts were centrifuged at 13000g, 4˚C for 10 minutes to remove cell debris. Protein concentrations were determined by Bradford assay (Thermo Scientific). Trehalase activity assays were performed immediately after extraction. 200 µl assay buffer (50 mM Tris buffer pH7, 50 uM $CaCl_2$, 100 mM trehalose) were pre-warmed to 30˚C and 20 µl extract were added to start the reaction. Samples and controls were incubated for 0, 30, or 60 minutes, respectively. To stop the reaction, samples were incubated in a 95˚C water bath for 3 minutes. Samples were centrifuged to remove protein debris and supernatants were stored at -20˚C until analysis. The glucose that was produced during the reaction was determined spectrophotometrically using a commercial enzyme kit (Megazymes).

Supplemental References

Koivomagi, M., Valk, E., Venta, R., Iofik, A., Lepiku, M., Balog, E.R.M., Rubin, S.M., Morgan, D.O., and Loog, M. (2011a). Cascades of multisite phosphorylation control Sic1 destruction at the onset of S phase. Nature *480*, 128-U301.

Yuan, J., Bennett, B.D., and Rabinowitz, J.D. (2008). Kinetic flux profiling for quantitation of cellular metabolic fluxes. Nat Protoc *3*, 1328-1340.